Elemental excitations in MoI$_3$ one-dimensional van der Waals nanowires EP

Fariborz Kargar, Zahra Barani, Nicholas R. Sesing, et al.

COLLECTIONS

Paper published as part of the special topic on Phononics of Graphene, Layered Materials, and Heterostructures

EP   This paper was selected as an Editor's Pick

View Online   Export Citation   CrossMark

ARTICLES YOU MAY BE INTERESTED IN

The effect of defect and substitution on barocaloric performance of neopentylglycol plastic crystals
Applied Physics Letters **121**, 223902 (2022); https://doi.org/10.1063/5.0131123

Emergence of considerable thermoelectric effect due to the addition of an underlayer in Pt/Co/Pt stack and its application in detecting field free magnetization switching
Applied Physics Letters **121**, 223502 (2022); https://doi.org/10.1063/5.0125607

Two-dimensional ferromagnetic materials: From materials to devices
Applied Physics Letters **121**, 220501 (2022); https://doi.org/10.1063/5.0130037

AIP Publishing

Elemental excitations in MoI₃ one-dimensional van der Waals nanowires (EP)

Fariborz Kargar,[1,a] (iD) Zahra Barani,[1] Nicholas R. Sesing,[2] (iD) Thuc T. Mai,[3] (iD) Topojit Debnath,[4] (iD)
Huairuo Zhang,[5,6] (iD) Yuhang Liu,[4] (iD) Yanbing Zhu,[7] Subhajit Ghosh,[1] (iD) Adam J. Biacchi,[8] (iD)
Felipe H. da Jornada,[9] (iD) Ludwig Bartels,[10] (iD) Tehseen Adel,[3] (iD) Angela R. Hight Walker,[3] (iD)
Albert V. Davydov,[6] (iD) Tina T. Salguero,[2] (iD) Roger K. Lake,[4] (iD) and Alexander A. Balandin[1,a] (iD)

AFFILIATIONS

[1]Nano-Device Laboratory (NDL) and Phonon Optimized Engineered Materials (POEM) Center, Department of Electrical
 and Computer Engineering, University of California, Riverside, California 92521, USA
[2]Department of Chemistry, University of Georgia, Athens, Georgia 30602, USA
[3]Quantum Measurement Division, Physical Measurement Laboratory, National Institute of Standards and Technology (NIST),
 Gaithersburg, Maryland 20899, USA
[4]Laboratory for Terascale and Terahertz Electronics (LATTE), Department of Electrical and Computer Engineering,
 University of California, Riverside, California 92521, USA
[5]Theiss Research, Inc., La Jolla, California 92037, USA
[6]Materials Science and Engineering Division, National Institute of Standards and Technology, Gaithersburg, Maryland 20899, USA
[7]Department of Applied Physics, Stanford University, Stanford, California 94305, USA
[8]Nanoscale Device Characterization Division, Physical Measurement Laboratory, National Institute of Standards and Technology
 (NIST), Gaithersburg, Maryland 20899, USA
[9]Department of Materials Science and Engineering, Stanford University, Stanford, California 94305, USA
[10]Department of Chemistry, University of California, Riverside, California 92521, USA

Note: This paper is part of the APL Special Collection on Phononics of Graphene, Layered Materials, and Heterostructures.
[a]Authors to whom correspondence should be addressed: fkargar@ece.ucr.edu and balandin@ece.ucr.edu.
URL: http://balandingroup.ucr.edu/

ABSTRACT

We report the polarization-dependent Raman spectra of exfoliated MoI₃, a van der Waals material with a "true one-dimensional" crystal structure that can be exfoliated to individual atomic chains. The temperature evolution of several Raman features reveals an anomalous behavior suggesting a phase transition of magnetic origin. Theoretical considerations indicate that MoI₃ is an easy-plane antiferromagnet with alternating spins along the dimerized chains and with inter-chain helical spin ordering. The calculated frequencies of phonons and magnons are consistent with the interpretation of the experimental Raman data. The obtained results shed light on the specifics of the phononic and magnonic states in MoI₃ and provide a strong motivation for further study of this unique material with potential for future spintronic applications.

Published under an exclusive license by AIP Publishing. https://doi.org/10.1063/5.0129904

A new research field focused on one-dimensional (1D) van der Waals (vdW) quantum materials has emerged from earlier works on low-dimensional systems.[1–4] The 1D vdW materials are based on 1D structural motifs and include transition metal trichalcogenides and halides.[1–5] It is helpful to distinguish true-1D vs quasi-1D vdW systems. We define the material to be true-1D if it contains only covalent bonds in the direction of the atomic chains with all other bonds being of vdW type; the material is quasi-1D if it contains strong covalent

bonds along the 1D chain direction while also bonded by weaker covalent bonds in the perpendicular planes. For example, according to this criterion, Nb₂Se₉ is a true-1D material whereas TaSe₃ is a quasi-1D material.[6–8] The number of vdW materials with quasi- or true-1D structures is not known, but machine learning investigations indicate that hundreds of 1D vdW materials are synthetically accessible.[5,9–11] True-1D vdW materials can be exfoliated chemically or mechanically into individual atomic chains or a few-atomic chain bundles.[2,6,12] One

can also envision that progress in chemical vapor deposition (CVD) will eventually allow the controlled synthesis of such 1D materials on substrates of choice, thereby enabling their practical applications.[13–15]

Owing to their unique dimensionality and electronic density of states, 1D materials often support unusual quasiparticle excitations, such as separated spin-charge excitations, Luttinger plasmons with quantized velocities,[16] magnetism,[17] charge density waves, and emergent topology.[18–21] Many of such unusual electronic properties also manifest themselves as nontrivial features in the dispersion relation of other collective excitations, such as phonons and magnons, due to their lower spatial dimensionality and stronger electronic correlation in 1D materials. The magnetic properties of 1D materials are of particular interest. The intrinsic ferromagnetic (FM) and antiferromagnetic (AFM) spin orderings are observed in the single atomic layers of some transition-metal dichalcogenides (MX_2) and transition-metal phospho-trichalcogenides (MPX_3) that constitute quasi-two-dimensional (2D) systems.[22,23] In these compositions, "M" is a transition metal, "X" is a chalcogen, and "P" is phosphorous. The possibility of AFM ordering in true-1D vdW materials is interesting from both fundamental science and practical application point of view. The prospect of the helical spin order, i.e., spin-spiral order, in 1D materials is particularly exciting.[24] The challenges with the experimental observation of magnetism in the 1D limit are complex owing to the scarcity of stable true-1D vdW material systems, the low signal-to-noise ratio in magnetometry and other related experiments, and difficulties in handling individual atomic chains. As a step in this direction, we use Raman spectroscopy to investigate the elemental excitations in exfoliated van der Waals nanowires of MoI_3, classified as a true-1D vdW material. While practical applications of such materials are in the distant future, one can envision that electrically insulating magnetic materials with the quasi-1D structure can serve as magnonic interconnects conducting pure spin currents in spintronic circuits.[25]

MoI_3 crystals for this study were prepared from the elements using the chemical vapor transport (CVT) technique.[12,26] The inclusion of NH_4I as a transport agent led to a more reliable synthetic procedure, likely due to lower internal ampule pressure and excellent product quality that allowed us to determine the single crystal structure of MoI_3 by x-ray diffraction; details and atomic coordinates are provided in the supplementary material (see Tables S1–S4 and Figs. S1 and S2). Figure 1(a) presents the crystal structure of MoI_3. Although this structure can be refined in both $Pmmn$ and $P6_3/mcm$ with low R values, we ultimately used $Pmmn$ in line with the interpretation of powder x-ray diffraction (PXRD) data by Ströbele and co-workers.[26] The $Pmmn$ structure was further confirmed by our high-angle annular dark-field scanning transmission electron microscopy (HAADF-STEM) imaging (vide infra). The space group selection is critical because $Pmmn$ leads to "dimerized" MoI_3 chains showing clear Peierls distortion with alternating Mo–Mo distances of 2.8793(19) and 3.5298(19) Å, whereas $P6_3/mcm$ leads to 1D chains of equidistant Mo atoms. We also validated the space group by PXRD; Fig. 1(b) shows the experimental pattern from MoI_3 crystals with selected hkl indices. (Complete hkl assignment is shown in Fig. S1 of the supplementary material.) Refined lattice parameters from the single crystal study [$a = 12.3183(4)$ Å, $b = 6.4091(2)$ Å, $c = 7.1180(3)$ Å] are similar to those from our PXRD analysis [$a = 12.3200(6)$ Å, $b = 6.4088(6)$ Å, $c = 7.1225(3)$ Å] as well as literature values.[26]
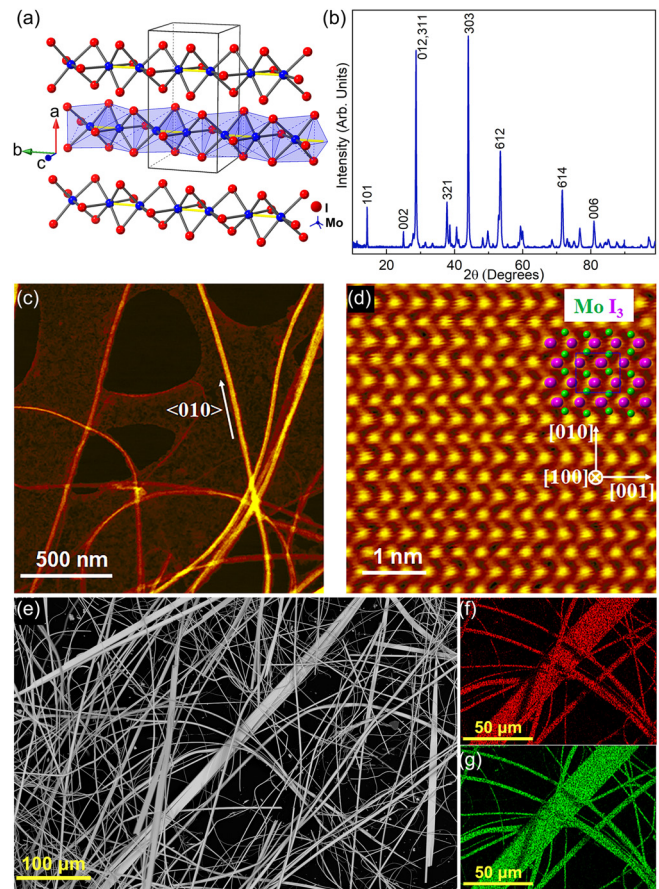
FIG. 1. (a) Crystal structure of MoI_3 refined in the $Pmmn$ (No. 59) space group; blue and red spheres represent Mo and I, respectively. The short Mo–Mo interactions of the dimerized MoI_3 chains are indicated with yellow bonds. (b) Experimental PXRD $\theta - 2\theta$ scan with selected hkl indices. (c) Low magnification HAADF-STEM image and (d) atomically resolved HAADF-STEM image of exfoliated MoI_3 nanowires. The images confirm the space group and show that the nanowires grow along the $\langle 010 \rangle$ direction. (e) SEM image of the as-synthesized MoI_3 crystals. (f) and (g) Corresponding EDS mapping that shows the uniform distribution of Mo (red) and I (green).

Figures 1(c) and 1(d) present the low-magnification HAADF-STEM and atomically resolved image of the exfoliated MoI_3 crystals, respectively. The latter confirms MoI_3 as the $Pmmn$ lattice structure along the (100) projection. Note that the scanning electron microscopy (SEM) image of representative MoI_3 crystals, presented in Fig. 1(e), shows that this material grows preferentially along the b-axis, leading to needlelike structures with high aspect ratios. The energy dispersive spectroscopy (EDS) mapping of the exfoliated samples shows a homogeneous distribution and overlap of Mo and I [Figs. 1(f) and 1(g)]. The EDS analytical results also confirm the expected composition of ∼1:3 Mo:I (see Table S5).

We used temperature- and polarization-dependent Raman spectroscopy to study the elemental excitations, i.e., phonons and magnons, in MoI_3 crystals. The experiments were conducted in the conventional backscattering configuration using a 488 nm laser excitation. In all experiments, the samples were positioned in such a way

that the polarization of the incident light was along the "b" crystallographic direction, i.e., along the nanowires. The polarization of the scattered light was selected to be either parallel with or transverse to the incident light. The power of the laser was kept at 400 μW to avoid self-heating effects. The results of the Raman measurements for the parallel and cross-polarization arrangements in the temperature range of 1.6–300 K are presented in Figs. 2(a) and 2(b), respectively. The unit cell of MoI_3 has 16 atoms with 45 optical phonon branches, resulting in a rich Raman response with many peaks in the range of 10–750 cm^{-1}. These Raman features strongly depend on the respective polarization of the incident and scattered light, which is typical for one-dimensional materials.[27,28] As theoretically shown later in this paper, the maximum energy of optical phonons and magnons in MoI_3 at the Brillouin zone (BZ) center is ~228 and ~310 cm^{-1}, respectively. Therefore, the peaks observed in the spectra above ~310 cm^{-1} are associated with the higher-order scattering processes, except the Si substrate peak at ~520 cm^{-1}. We plotted the spectral position and full-width-at-half-maximum (FWHM) of three well-defined peaks, labeled as "p_1," "p_2," and "p_3" [Fig. 2(a)], as a function of temperature. These peaks have A_g, B_1g, and B_3g vibrational symmetries. The results are presented in Figs. 2(c) and 2(d).

Generally, the phonon features in Raman spectra of different materials shift to lower frequencies with increasing temperature, which is explained by the crystal lattice expansion and phonon anharmonic effects.[29] This is the case for the Raman peak p_3 at ~210 cm^{-1}. The spectral positions of the other two peaks at ~57 and ~88 cm^{-1} blue-shift with increasing temperature. Phonon hardening with increasing temperature, observed for the peaks labeled as p_1 and p_2, is unusual. Similar anomalous behavior has been previously reported for the so-called soft phonon modes in ferroelectric materials such as $SrTiO_3$, the transverse acoustic modes in Invar alloys, and magnetic random solid solutions such as $Fe_{1-x}Pd_x$.[30,31] In the latter case, the phonon hardening was attributed to thermal magnetic fluctuations.[32] One can further notice a deviation in the FWHM temperature dependence from a linear behavior with a pronounced kink at ~150 K for both Raman features (p_1 and p_2). Such a non-monotonic characteristic of FWHM could indicate a magnetic phase transition in MoI_3.

The intensity of the peaks associated with scattering processes involving magnons tends to weaken with temperature and eventually fall to zero beyond the magnetic phase transition temperature.[33] One can see in Figs. 2(a) and 2(b) that the intensity decreases for all peaks with increasing temperature, leaving the task of distinguishing
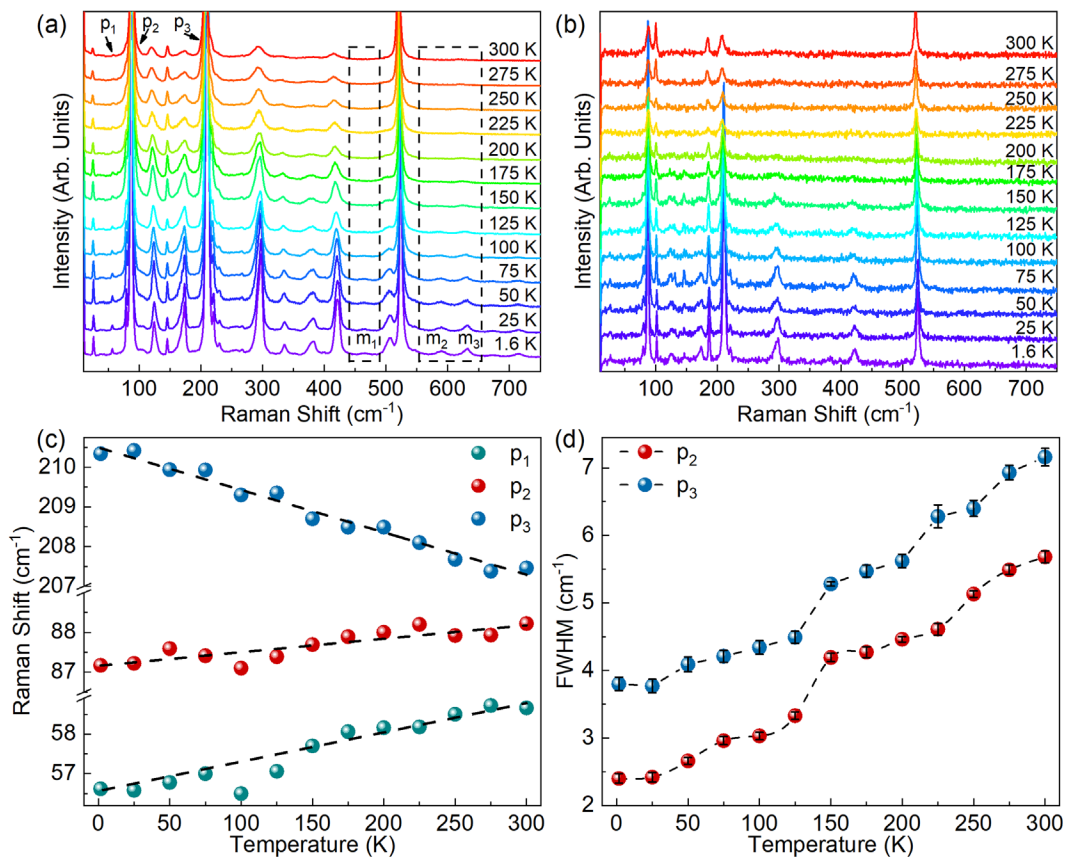
FIG. 2. Evolution of the (a) parallel and (b) cross-polarization Raman spectra excited with 488 nm excitation as a function of temperature. The polarization of the incident light is along the nanowires. The dashed rectangular shows the high-frequency feature assigned to the two-magnon scattering process. (c) Spectral position of the peaks labeled as p_1, p_2, and p_3 in panel (b). (d) FWHM of the intense p_2 and p_3 Raman peaks at ~88 and 207 cm^{-1} as a function of temperature. Note the abrupt increase in the FWHM of both peaks at 150 K.

possible magnon peaks from phonon peaks extremely difficult. It should be noted that the spectral position of the peaks is insensitive to the magnetic field of 9 T applied along the crystal's "c" axis as well. Yet, this does not exclude the possibility of magnetic order. It is known that in many AFM materials, e.g., NiO, even a strong magnetic field produces small effects on the Raman spectrum.[34] Three broad Raman features at ~465, ~580, and ~625 cm^{-1} (labeled as "m$_1$," "m$_2$," and "m$_3$") encompassed by the rectangular dashed lines in Fig. 2(a) contain additional valuable information. The theory described below indicates that these spectral features are associated with two-magnon scattering processes. They disappear completely in the temperature range from 125 to 150 K, and their energy exactly matches the calculated magnon energy at the BZ edge along the $\Gamma - Y$ direction, multiplied by a factor of two, as it should be for the two-magnon processes.

To further elucidate the nature of the observed phase transition in MoI$_3$, we plot the intensity color map of the Raman spectra shown in Fig. 2(a) as a function of the temperature and frequency in the low and high wavenumber regions. The results are presented in Figs. 3(a) and 3(b). The difference in the intensity of the Raman peaks in these two frequency ranges is significant; the latter explains the reason for plotting them separately. In both plots, the color change from violet to red indicates the peaks become more intense. The white regions in Figs. 3(a) and 3(b) are the strong peaks at 88 and 207 cm^{-1} and the Si
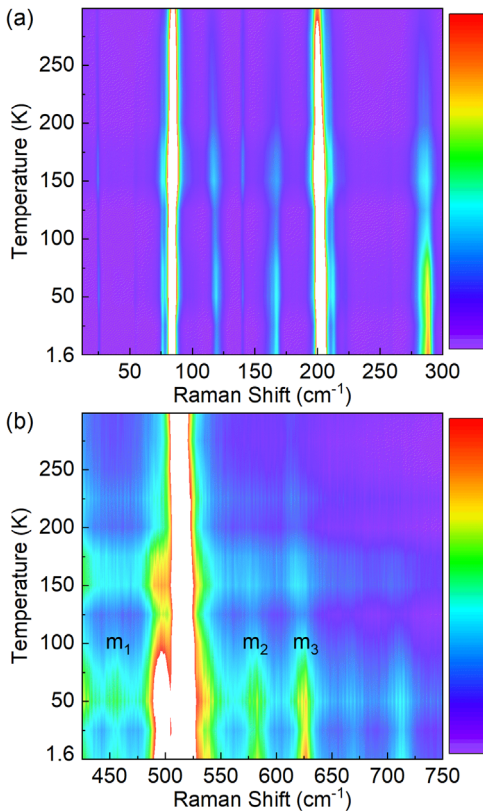

FIG. 3. The intensity colormap of the Raman spectra accumulated in the parallel-polarization configuration. The spectra are presented for the (a) low and (b) high wavenumber ranges for clarity. Note that the intensity of the m$_1$, m$_2$, and m$_3$ peaks attributed to the two-magnon scattering gradually disappears at T ∼ 200 K.

peak at 520 cm^{-1} [see Fig. 2(a)]. They are shown with white color because their intensity is beyond the defined maximum level in the colormap (the red color) to avoid overshadowing the weak features of interest. One can see in Fig. 3(a) that none of the peaks has its intensity vanishing as the temperature rises. This confirms that all these peaks are associated with the phonon scattering processes. Interestingly, the broad Raman features at 465, 580, and 625 cm^{-1} completely vanish at the same temperature range. Similar broad features associated with the two-magnon scattering processes are common in AFM materials such as MnF$_2$, NiO$_2$, MnPSe$_3$, and VI$_3$.[35–38]

A recent study predicted the AFM spin-ordering in MoI$_3$ using machine learning algorithms.[5] This report did not describe the specific type of AFM ordering or the Néel temperature of the transition in MoI$_3$. To compare directly the theory prediction with our experimental results, we performed *ab initio* calculations of the phonon and magnon dispersion of MoI$_3$. Density functional theory (DFT) calculations were carried out with the generalized gradient approximation (GGA)[39] exchange-correlation functional of Perdew, Burke, and Ernzerhof (PBE)[40,41] as implemented in the Vienna *ab initio* simulation package (VASP).[42] The ion–electron interactions use the projected augmented wave (PAW) method. The energy cutoff for the plane wave basis was set to 520 eV. All the structures were allowed to relax during this process with a conjugate gradient algorithm until the energy on the atoms was less than 10^{-4} eV. The DFT-D3 approach proposed by Grimme[43] was used for the vdW interactions. A Hubbard + U value of 4.0 was used on the Mo atoms. This value was found to minimize the negative modes in the phonon dispersion. Phonon calculations were performed using the finite-displacement supercell approach as implemented in Phonopy.[44,45] For the phonon calculations, the Brillouin zone was sampled by a $4 \times 7 \times 4$ Monkhorst–Pack k-point grid. The results of the calculations are presented in Fig. 4(a). The green spheres are the spectral position of Raman peaks in the range of 10–250 cm^{-1} in the parallel polarization configuration [see Fig. 2(a)]. The theoretical calculations are in excellent agreement with the experimental data.

The magnetic properties were calculated with PBE + U, as described above, with the inclusion of spin–orbit coupling (SOC). To determine the magnetic ground state, total energy calculations were performed with the magnetic moments of the Mo atoms in ferromagnetic (FM) order and two different anti-ferromagnetic (AFM) orders (see Fig. S3 in the supplementary material). The ground state energy of the FM order was approximately 1.5 eV higher per unit cell than the ground state energies of the two different AFM configurations. In both AFM configurations, alternating spins were anti-aligned along the chains. From total energy calculations with different spin configurations, the exchange coupling constants and the magnetic anisotropy energy (MAE) were determined for the magnetic Hamiltonian given by the following equation:

$$H_m = \sum_{\alpha m \neq \beta m} J_{\alpha m;\beta n}\, \boldsymbol{S}_{\alpha m} \cdot \boldsymbol{S}_{\beta n} + \sum_{\alpha m} A\left(S_{\alpha m}^y\right)^2 + g\mu_B \sum_{\alpha m} \boldsymbol{B} \cdot \boldsymbol{S}_{\alpha m}. \quad (1)$$

Here, greek indices label the different chains, and Roman indices label the atoms within the chain. There are three non-zero values for the exchange constants $J_{\alpha m;\beta n}$. Within the same chain, $J_1 = 187$ and $J_2 = 0.884$ meV are the exchange couplings corresponding to the shorter Mo–Mo distance and longer Mo–Mo distance, respectively, as illustrated in Fig. 4(b). $J_3 = 0.119$ meV is the exchange coupling
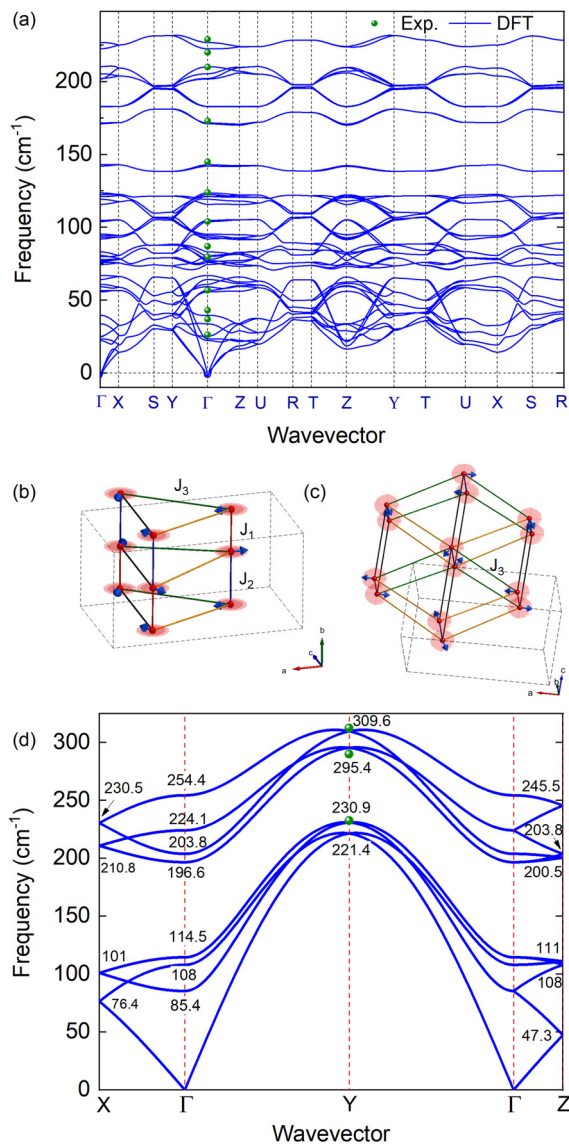
FIG. 4. (a) Calculated phonon dispersion in blue with the experimental peaks shown by the green spheres. (b) Triangular arrangement of chains with 120° rotation of spins between nearest neighbor chains. (c) Dimerized chains illustrating the two different intra-chain exchange constants, J_1 and J_2, and the inter-chain exchange constant J_3. The red circles indicate the easy plane of magnetic anisotropy. (d) Calculated magnon dispersion with the frequencies at high symmetry points shown. The green spheres are the experimental data points.

between Mo atoms in the same plane on different chains, as illustrated in Figs. 4(b) and 4(c). All exchange terms are positive. The positive magnetic anisotropy energy (MAE) $A = 0.17$ meV causes the spins to lie in the a–c plane perpendicular to the chain direction. Magnetic anisotropy within the a–c plane is too small to be resolved from our DFT calculations. The third term of the Hamiltonian is the external magnetic field. MoI_3 consists of dimerized AFM chains arranged in a triangular lattice as shown in Figs. 4(b) and 4(c). Total energy

calculations based on the magnetic Hamiltonian of Eq. (1) found that the chain-to-chain spins in the same plane form spin-spirals with 120° rotation angles between chains, typical of a triangular lattice. The magnon dispersion for bulk MoI_3 was calculated from Eq. (1) using the linear spin wave theory as implemented in SpinW[46] and is shown in Fig. 4(d). The numbers in this plot are the frequencies of different magnon branches at high symmetry points. The green spheres are the experimental spectral position of the two-magnon Raman peaks shown in Fig. 3(b) divided by two. The frequency of the two-magnon peaks exactly matches the energy of the magnon branches at the BZ edge along the $\Gamma - Y$ direction. We can state that the theory of the phonon and magnon states in this true-1D vdW material is consistent with our experimental Raman data.

We also theoretically considered the effects of an external applied magnetic field on the magnon dispersion. By introducing a magnetic field of 10 T in the theory, we observed that the bands at the gamma point are split by a small value of $\sim$0.5 cm^{-1}, which was not present in the dispersion without the field. The experimental efforts to detect this difference in the energies of the split bands were not conclusive as these calculated frequency differences are at the limit of the instrumental resolution of our Raman systems. The Raman spectra collected under a magnetic field of 9 T at 1.6 K do not exhibit any pronounced changes in the spectral position of the peaks nor any splitting of the magnon peaks. It is important to emphasize again that the phonon dispersion calculations are in excellent agreement with the experimentally measured spectral position of the peaks at the Γ point. Our preliminary magnetometry data reveal a weak signal. This can be attributed to the difficulty in the measurements of the exfoliated nanowires. Further studies are needed with larger quantities of the material for a direct comparison of magnetometry and Raman data.

In summary, we described here the elemental excitations in crystals of MoI_3, a vdW material with a true-1D crystal structure. Our measurements reveal anomalous temperature dependence of the Raman spectral features of MoI_3, which suggest magnetic phase transitions. The theoretical calculations of the phonon and magnon dispersion are in excellent agreement with the experimental data. The magnon zone-edge frequencies are consistent with the interpretation of the Raman data and the assignment of the two-magnon scattering. The results shed light on the phononic and magnonic properties of 1D MoI_3 nanowires and provide a strong motivation for future study of this unique material.

See the supplementary material for additional data on material synthesis and characterization.

Certain commercial equipment, instruments, software, or materials are identified in this paper in order to specify the experimental procedure adequately. Such identifications are not intended to imply recommendation or endorsement by NIST, nor is it intended to imply that the materials or equipment identified are necessarily the best available for the purpose.

AUTHOR DECLARATIONS
Conflict of Interest

The authors have no conflicts to disclose.

Author Contributions

Alexander A. Balandin and Fariborz Kargar: conceived the idea, coordinated the project, contributed to experimental data analysis, and led the manuscript preparation. Nicholas R. Sesing synthesized bulk crystals by CVT. Tina T. Salguero supervised material synthesis and contributed to data analysis. Zahra Barani, Thuc Tan Mai, and Tehseen Adel conducted Raman spectroscopy studies at UCR and NIST. Huairuo Zhang conducted the TEM characterization; Angela R. Hight Walker and Albert V. Davydov supervised material characterization and contributed to data analysis. Topojit Debnath, Yuhang Liu, and Yanbing Zhu conducted *ab initio* simulations of the phonon and magnon dispersion at UCR and Stanford, respectively. Felipe da Jornada and Roger K. Lake contributed to the data analysis and supervised the simulations. Ludwig Bartels, Subhajit Ghosh, and Adam J. Biacchi contributed to the data analysis. All authors contributed to the manuscript preparation and editing. Tina T. Salguero and Albert V. Davydov thank Dr. Pingrong Wei (UGA) and Dr. Sergiy Krylyuk (NIST) for assistance with the single crystal and powder x-ray diffraction study.

DATA AVAILABILITY

The data that support the findings of this study are available from the corresponding author upon reasonable request.

REFERENCES

[1] A. A. Balandin, R. K. Lake, and T. T. Salguero, Appl. Phys. Lett. **121**, 040401 (2022).

[2] A. A. Balandin, F. Kargar, T. T. Salguero, and R. K. Lake, Mater. Today **55**, 74 (2022).

[3] J. K. Qin, C. Wang, L. Zhen, L. J. Li, C. Y. Xu, and Y. Chai, Prog. Mater. Sci. **122**, 100856 (2021).

[4] J. O. Island, A. J. Molina-Mendoza, M. Barawi, R. Biele, E. Flores, J. M. Clamagirand, J. R. Ares, C. Sánchez, H. S. J. van der Zant, R. D'Agosta, I. J. Ferrer, and A. Castellanos-Gomez, 2D Mater. **4**, 022003 (2017).

[5] L. Fu, C. Shang, S. Zhou, Y. Guo, and J. Zhao, Appl. Phys. Lett. **120**, 023103 (2022).

[6] S. Oh, S. Chae, B. J. Kim, A. J. Siddiqa, K. H. Choi, W. S. Jang, K. H. Lee, H. Y. Kim, D. K. Lee, Y. M. Kim, H. K. Yu, and J. Y. Choi, Phys. Status Solidi RRL **12**, 1800451 (2018).

[7] Z. Barani, F. Kargar, Y. Ghafouri, S. Ghosh, K. Godziszewski, S. Baraghani, Y. Yashchyshyn, G. Cywiński, S. Rumyantsev, T. T. Salguero, and A. A. Balandin, Adv. Mater. **33**, 2007286 (2021).

[8] F. Kargar, A. Krayev, M. Wurch, Y. Ghafouri, T. Debnath, D. Wickramaratne, T. T. Salguero, R. K. Lake, L. Bartels, and A. A. Balandin, Nanoscale **14**, 6133 (2022).

[9] G. Cheon, K.-A. N. Duerloo, A. D. Sendek, C. Porter, Y. Chen, and E. J. Reed, Nano Lett. **17**, 1915 (2017).

[10] G. Cheon, E. D. Cubuk, E. R. Antoniuk, L. Blumberg, J. E. Goldberger, and E. J. Reed, J. Phys. Chem. Lett. **9**, 6967 (2018).

[11] Y. Zhu, D. A. Rehn, E. R. Antoniuk, G. Cheon, R. Freitas, A. Krishnapriyan, and E. J. Reed, ACS Nano **15**, 9851 (2021).

[12] K. H. Choi, S. Oh, S. Chae, B. J. Jeong, B. J. Kim, J. Jeon, S. H. Lee, S. O. Yoon, C. Woo, X. Dong, A. Ghulam, C. Lim, Z. Liu, C. Wang, A. Junaid, J. H. Lee, H. K. Yu, and J. Y. Choi, J. Alloys Compd. **853**, 157375 (2021).

[13] M. Sun, J. Li, Q. Ji, Y. Lin, J. Wang, C. Su, M. H. Chiu, Y. Sun, H. Si, T. Palacios, J. Lu, D. Xie, and J. Kong, Phys. Rev. Mater. **5**, 94002 (2021).

[14] T. A. Empante, A. Martinez, M. Wurch, Y. Zhu, A. K. Geremew, K. Yamaguchi, M. Isarraraz, S. Rumyantsev, E. J. Reed, A. A. Balandin, and L. Bartels, Nano Lett. **19**, 4355 (2019).

[15] J. Jin, M. Wurch, S. Baraghani, D. J. Coyle, T. A. Empante, F. Kargar, A. A. Balandin, and L. Bartels, Cryst. Growth Des. **21**, 6537 (2021).

[16] Z. Shi, X. Hong, H. A. Bechtel, B. Zeng, M. C. Martin, K. Watanabe, T. Taniguchi, Y. R. Shen, and F. Wang, Nat. Photonics **9**, 515 (2015).

[17] Y. W. Son, M. L. Cohen, and S. G. Louie, Nature **444**, 347 (2006).

[18] W. Shi, B. J. Wieder, H. L. Meyerheim, Y. Sun, Y. Zhang, Y. Li, L. Shen, Y. Qi, L. Yang, J. Jena, P. Werner, K. Koepernik, S. Parkin, Y. Chen, C. Felser, B. A. Bernevig, and Z. Wang, Nat. Phys. **17**, 381 (2021).

[19] A. A. Balandin, S. V. Zaitsev-Zotov, and G. Grüner, Appl. Phys. Lett. **119**, 170401 (2021).

[20] G. Grüner, Rev. Mod. Phys. **60**, 1129 (1988).

[21] J. Li, S. Sanz, N. Merino-Díez, M. Vilas-Varela, A. Garcia-Lekue, M. Corso, D. G. de Oteyza, T. Frederiksen, D. Peña, and J. I. Pascual, Nat. Commun. **12**, 5538 (2021).

[22] M. Bonilla, S. Kolekar, Y. Ma, H. C. Diaz, V. Kalappattil, R. Das, T. Eggers, H. R. Gutierrez, M. H. Phan, and M. Batzill, Nat. Nanotechnol. **13**, 289 (2018).

[23] D. J. O'Hara, T. Zhu, A. H. Trout, A. S. Ahmed, Y. K. Luo, C. H. Lee, M. R. Brenner, S. Rajan, J. A. Gupta, D. W. McComb, and R. K. Kawakami, Nano Lett. **18**, 3125 (2018).

[24] I. A. Golovchanskiy and V. S. Stolyarov, J. Appl. Phys. **131**, 53901 (2022).

[25] A. V. Chumak, V. I. Vasyuchka, A. A. Serga, and B. Hillebrands, Nat. Phys. **11**, 453 (2015).

[26] M. Ströbele, R. Thalwitzer, and H. J. Meyer, Inorg. Chem. **55**, 12074 (2016).

[27] T. J. Wieting, A. Grisel, and F. Levy, in *Molecular Crystals and Liquid Crystals* (Taylor & Francis Group, 1982), pp. 117–124.

[28] W. Kong, C. Bacaksiz, B. Chen, K. Wu, M. Blei, X. Fan, Y. Shen, H. Sahin, D. Wright, D. S. Narang, and S. Tongay, Nanoscale **9**, 4175 (2017).

[29] S. Zhu and W. Zheng, J. Phys. Chem. Lett. **12**, 5261–5270 (2021).

[30] I. A. Akimov, A. A. Sirenko, A. M. Clark, J.-H. Hao, and X. X. Xi, Phys. Rev. Lett. **84**, 4625 (2000).

[31] B. Sato, M. Grier, S. Shapiro, and H. Miyajima, J. Phys. F **12**, 2117 (1982).

[32] Y. Ikeda, F. Körmann, B. Dutta, A. Carreras, A. Seko, J. Neugebauer, and I. Tanaka, npj Comput. Mater. **4**, 1 (2018).

[33] A. McCreary, J. R. Simpson, T. T. Mai, R. D. McMichael, J. E. Douglas, N. Butch, C. Dennis, R. V. Aguilar, and A. R. Hight Walker, Phys. Rev. B **101**, 064416 (2020).

[34] J. Milano and M. Grimsditch, Phys. Rev. B **81**, 094415 (2010).

[35] E. Aytan, B. Debnath, F. Kargar, Y. Barlas, M. M. Lacerda, J. X. Li, R. K. Lake, J. Shi, and A. A. Balandin, Appl. Phys. Lett. **111**, 252402 (2017).

[36] B. Lyu, Y. Gao, Y. Zhang, L. Wang, X. Wu, Y. Chen, J. Zhang, G. Li, Q. Huang, N. Zhang, Y. Chen, J. Mei, H. Yan, Y. Zhao, L. Huang, and M. Huang, Nano Lett. **20**, 6024 (2020).

[37] M. G. Cottam and D. J. Lockwood, J. Magn. Magn. Mater. **54–57**, 1143 (1986).

[38] T. T. Mai, K. F. Garrity, A. McCreary, J. Argo, J. R. Simpson, V. Doan-Nguyen, R. V. Aguilar, and A. R. Hight Walker, Sci. Adv. **7**, 3106 (2021).

[39] J. P. Perdew, K. Burke, and M. Ernzerhof, Phys. Rev. Lett. **77**, 3865 (1996).

[40] P. E. Blochl, Phys. Rev. B **50**, 17953 (1994).

[41]G. Kresse and D. Joubert, Phys. Rev. B **59**, 1758 (1999).

[42]G. Kresse and J. Furthmüller, Comput. Mater. Sci. **6**, 15 (1996).

[43]S. Grimme, J. Antony, S. Ehrlich, and H. Krieg, J. Chem. Phys. **132**, 154104 (2010).

[44]A. Togo, F. Oba, and I. Tanaka, Phys. Rev. B. **78**, 134106 (2008).

[45]A. Togo and I. Tanaka, Scr. Mater. **108**, 1 (2015).

[46]S. Toth and B. Lake, J. Phys. **27**, 166002 (2015).